Experimental and theoretical investigations of a laser-produced aluminum plasma

S. Gurlui,[1] M. Agop,[2] P. Nica,[2] M. Ziskind,[3] and C. Focsa[3]
[1]*Faculty of Physics, "Al. I. Cuza" University, Boulevard Carol I no. 11, Iasi 700506, Romania*
[2]*Department of Physics, Technical "Gh. Asachi" University, Boulevard Mangeron no. 64, Iasi 700029, Romania*
[3]*Laboratoire de Physique des Lasers, Atomes et Molécules (UMR 8523), Centre d'Etudes et de Recherches Lasers et Applications (FR CNRS 2416), Université des Sciences et Technologies de Lille, 59655 Villeneuve d'Ascq cedex, France*
(Received 1 November 2007; revised manuscript received 6 April 2008; published 13 August 2008)

The formation and dynamics of a laser-produced aluminum plasma have been experimentally and theoretically investigated. The visible-emitting regions of the plasma form two structures with different lifetimes and expansion velocities. The first part of the transient ionic signal simultaneously recorded by a Langmuir probe presents an oscillatory structure. A hydrodynamic model in a nondifferentiable space-time has been established. The numerical simulation of the plasma expansion showed the plasma plume separation into two patterns. Moreover, the self-structuring of the interface appears through a negative differential conductance and the current oscillations are explained as being induced by thermal fluctuations that appear in the plasma cooling processes.

DOI: 10.1103/PhysRevE.78.026405 PACS number(s): 52.38.Mf, 52.30.−q, 47.53.+n, 52.65.−y

I. INTRODUCTION

For a number of experiments involving the interaction of intense laser pulses with matter, it is desirable to know the directionality, velocity, and other parameters of ejected plasma far from the target. Laser film deposition [1], laser-induced breakdown spectroscopy [2], and material processing [3,4] can be viewed as typical applications. A variety of physical processes, for instance laser-material interaction, hydrodynamics, thermal and radiative transport, make analytical description extremely difficult. In this case, numerical simulations are the only viable option. However, the large disparity in spatial and temporal scales involved often makes it impractical to simulate both ablation and plasma expansion to large distances from the target within the framework of one model. For example, a typical calculation would require an adequate description of laser energy deposition which occurs on a time scale of tens of nanoseconds and on a spatial scale on the order of micrometers. Plume modeling has to predict behavior of the plasma at the final stage of expansion that takes place microseconds and centimeters away from the initial event.

According to [5], a possible solution to this problem is to employ more than one model, each suitable for a particular stage, and match them at an intermediate time. Plume evolution includes two important parts—the initial stage is one dimensional (laser spot large compared to skin depth) and the final one consists of three-dimensional expansion [6–10]. The difference is not only geometrical; in the physics it plays the major, defining role. The initial one-dimensional stage occurs during laser energy deposition followed by the very first moments of the expansion. The longitudinal size of the hot material is still much smaller than the transverse size determined by the laser spot. Clearly, laser-material interaction, ionization, energy, and material transport are the significant effects during this period. After some time, the plasma cloud becomes truly three dimensional, but the physics simplifies considerably. At this stage, plume evolution is described by conventional hydrodynamics and is sensitive only to integral parameters of the laser pulse.

According to [6–11], both the elementary physical processes, which require different scale times, and the pattern evolution [12], which requires different degrees of freedom (e.g. from one, at the initial stages, to three, at the final stages of the patterns induced by the laser-produced plasma), imply a nondifferentiable space-time, i.e., fractals [13–15]. This means that the physical parameters are scale dependent and in such a context the scale relativity model has been developed [16]. As an example, the study of the anodic patterns in plasma discharges is one application of this theory [11].

A fractal structure is a manifestation of the universality of self-organization processes in plasma expansion [12], a result of a sequence of spontaneous symmetry-breaking processes [17,18]. Then, a cascade self-organization scenario of the pattern genesis and evolution can be admitted [19]. Also, the dynamics of the transition of plasma from "disorder" to "order" needs a different type of description: the fractal one. This paper attempts to build a dynamics of the "multiparticle" systems on a fractal space-time. The model is applied to the study of an expanding aluminum plasma produced by laser ablation.

II. EXPERIMENTAL SETUP

The experimental technique is based on a setup (see Fig. 1 for a schematic view) developed mainly for analytical purposes and described in detail elsewhere [20,21]. The experiments were performed in a stainless steel vacuum chamber evacuated by means of a 450 l/s turbomolecular pump to a base pressure below 10^{-6} Torr. A 10 ns neodymium-doped yttrium aluminum garnet (Nd:YAG) pulsed laser beam ($\lambda = 532$ nm) was focused by an $f=25$ cm lens on an aluminum target placed in the vacuum chamber. The estimated spot diameter at the impact point was ~ 300 μm. The laser beam energy (1–100 mJ/pulse) was continuously monitored by an OPHIR joulemeter. The energy usually employed was ~ 40 mJ/pulse; this leads to a typical laser intensity of ~ 5.7 GW/cm^2.

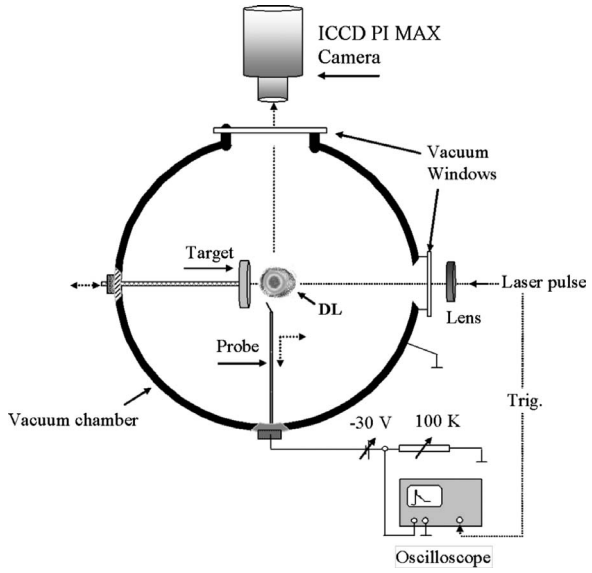

FIG. 1. Schematic view of the experimental setup.

The formation and dynamics of the plasma plume have been studied by means of an intensified charge-coupled device (ICCD) camera (PI MAX, 576X384 pixels, gating time 20 ns) placed orthogonal to the plasma expansion direction. A Nikon lens was used to image the plume onto the camera.

The total ionic current generated by the plasma expansion was measured by a cylindrical Langmuir probe (stainless steel, 0.8 mm diameter, 5 mm length), biased at −30 V (stabilized dc power source) and placed at various positions in the plasma plume (see below for details). The transitory signals were recorded by a 500 MHz digital oscilloscope (LeCroy 9350AM) and transferred to a PC for further analysis (LABVIEW environment).

III. EXPERIMENTAL RESULTS

In Fig. 2 the ICCD images of the expanding aluminum plasma plume at different delays after the laser pulse are given. The images of these structures reveal a splitting process of the plasma blobs into fast and slower parts. According to [12], the two well-localized plasma patterns have an electric double-layer structure. By analyzing the evolution presented in Fig. 2, we conclude the followings (i) In the time interval 10–50 ns after the laser pulse, the visible-emitting regions of the plasma are almost stationary and they form two structures, each of them having a maximum emissive zone (see marks I and II). (ii) After this moment, the first emitting structure flies away and eventually disappears, having an estimated lifetime of ~400 ns (iii) Behind the first plasma structure, a second (almost spherical) one is formed and its lifetime is about 1500 ns. It was experimentally observed that this lifetime strongly depends on the laser beam energy. Note that the separation of the two structures takes place on a very short time scale, typically of the order of the laser pulse duration. Such short phase explosion nucleation time lags (5 ns) have already been demonstrated theoretically and experimentally in nanosecond laser ablation with comparable fluences [22–24].

Using experimental data from optical diagnosis, the velocities of the two plasma formations have been calculated by measuring the position of the maximum emissivity at different times. The results are given in Fig. 3. The experimental data were fitted by linear regression and the velocities of the two structures have been estimated. We obtained $v_1 = 4.66 \times 10^4$ m/s for the first plasma structure [Fig. 3(a)] and $v_2 = 6.9 \times 10^3$ m/s for the second one [Fig. 3(b)].

The transient ionic currents recorded by the Langmuir probe for various laser beam energies are plotted in Fig. 4(a), and detailed in Fig. 4(b) for the laser energy of 40 mJ/pulse. For these measurements, the probe was located on the expanding plasma symmetry axis (z), at $z=18.5$ mm from the target surface Analyzing these profiles, we obtained the following results. (i) The current recorded by the Langmuir probe has a multipeak structure. In the region of the probe, the previous two plasma structures are evidenced as two arrival times. Thus, the first part of the transient signal takes about 2 μs and has an oscillatory structure with the average period of 240 ns, which does not depend on the laser energy [see Fig. 4(a)]. However, for laser energies lower than 2.5 mJ, such an oscillatory structure was not observed. The arrival time of the first ionic peak ranges between 200 and 300 ns and strongly depends on the laser energy. The second part of the ionic transient signal shows a distribution with a maximum at about 3000 ns [see Fig. 4(b)]. (ii) The results obtained by the electrical probe are in good agreement with those recorded by optical methods. As is seen in Fig. 4(b), for the laser beam energy 40 mJ, the ionic current obtained by electrical methods has its maximum at 250 ns, that is, in concordance with the arrival time of the maximum intensity of 200–300 ns shown in Fig. 2 (see the position of the Langmuir probe located on the normal to the target at $z=18.5$ mm). Moreover, taking into account the velocity of the second structure [Fig. 3(b)], this means reaching the Langmuir probe after $t=[18.5\times10^{-3}(\mathrm{m})]/[6.9\times10^{3}(\mathrm{m/s})] = 2700$ ns, which is in good agreement with the result indicated by the Langmuir probe signal.

More detailed measurements of the ionic current oscillations are given in Figs. 4(c) and 4(d). It results that this feature is preserved by changing the position of the Langmuir probe vs the z distance on the normal to the target [Fig. 4(c)] or by keeping constant this distance and modifying the radial distance (r) to the symmetry expansion axis [Fig. 4(d)]. However, in this last case the current oscillation disappears for $r>10$ mm, i.e., at large radial distance. Although surprising at first sight, the occurrence of such oscillations in the laser ablation plumes has already been shown [25] and is usually explained by plasma double-layer effects.

IV. FRACTAL HYDRODYNAMIC MODEL

Let us suppose that the motion of plasma particles takes place on continuous but nondifferentiable curves, i.e., on fractals [16]. The "nondifferentiability" in the topological dimension $D_T=2$ [13–16] implies the replacement of the standard time derivative d/dt by a new complex operator δ/dt [11,16],

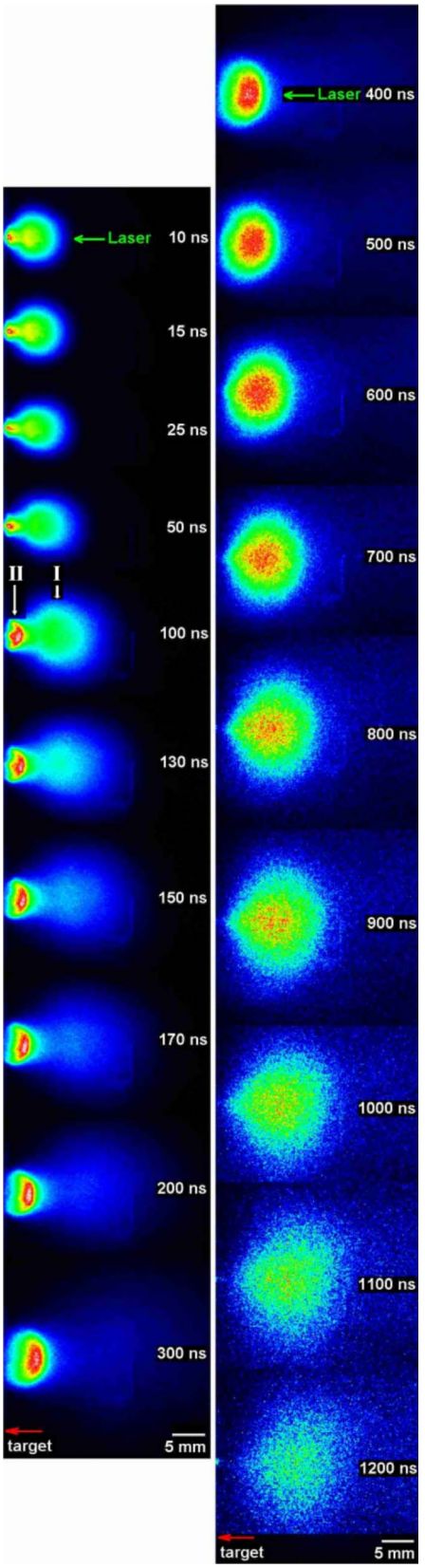

FIG. 2. (Color online) Evolution of the visible emission from the aluminum plasma plume recorded using an ICCD PI MAX camera (gating time 20 ns). The marks I and II show the plasma plume splitting. Successive laser pulses of equal energy (40 mJ/pulse) were used to record the different shots.

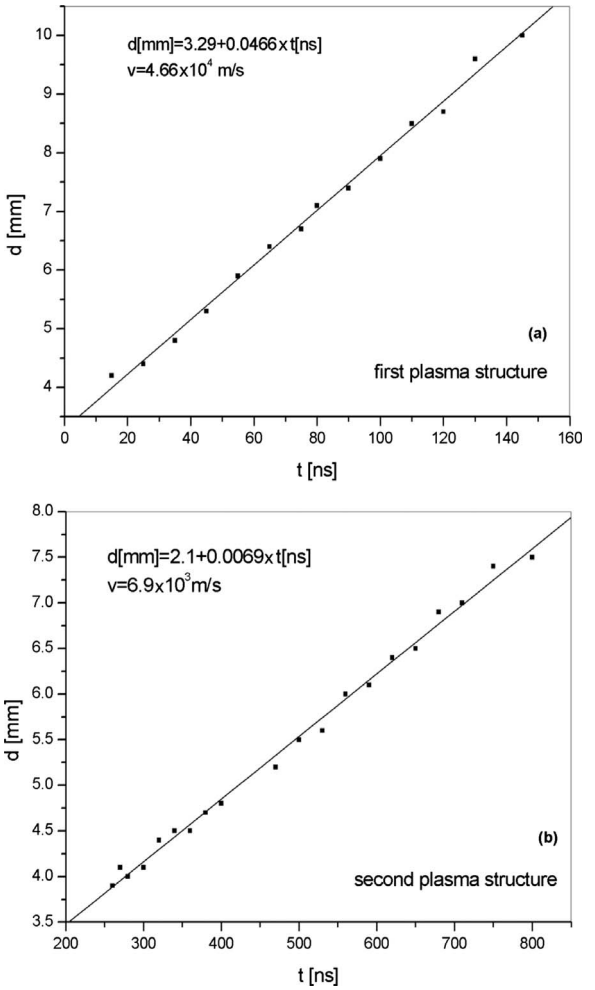

FIG. 3. Expansion velocities of the first (a) and second (b) plasma structures. The position of the maximum emission region is plotted against the delay after the laser pulse.

$$\frac{\delta}{dt} = \frac{\partial}{\partial t} + \boldsymbol{V}\cdot\boldsymbol{\nabla} - iD\Delta,$$

where $\boldsymbol{V}$ is the complex speed field and D defines the fractal-nonfractal transition, i.e., the transition from explicit scale dependence to scale independence (Nottale's coefficient [16]). As a consequence, the covariant form of the first Newtonian principle in the nondifferentiable space-time is reduced to a generalized Navier-Stokes-type equation,

$$\frac{\delta \boldsymbol{V}}{dt} = \frac{\partial \boldsymbol{V}}{\partial t} + \boldsymbol{V}\cdot\boldsymbol{\nabla}\boldsymbol{V} - iD\Delta\boldsymbol{V} = \boldsymbol{0}. \quad (1)$$

If the plasma is irrotational, $\boldsymbol{\Omega} = \boldsymbol{\nabla}\times\boldsymbol{V} = \boldsymbol{0}$, we can choose $\boldsymbol{V}$ of the form:

$$\boldsymbol{V} = -2iD\,\boldsymbol{\nabla}(\ln\psi). \quad (2)$$

Then, Eq. (1) becomes

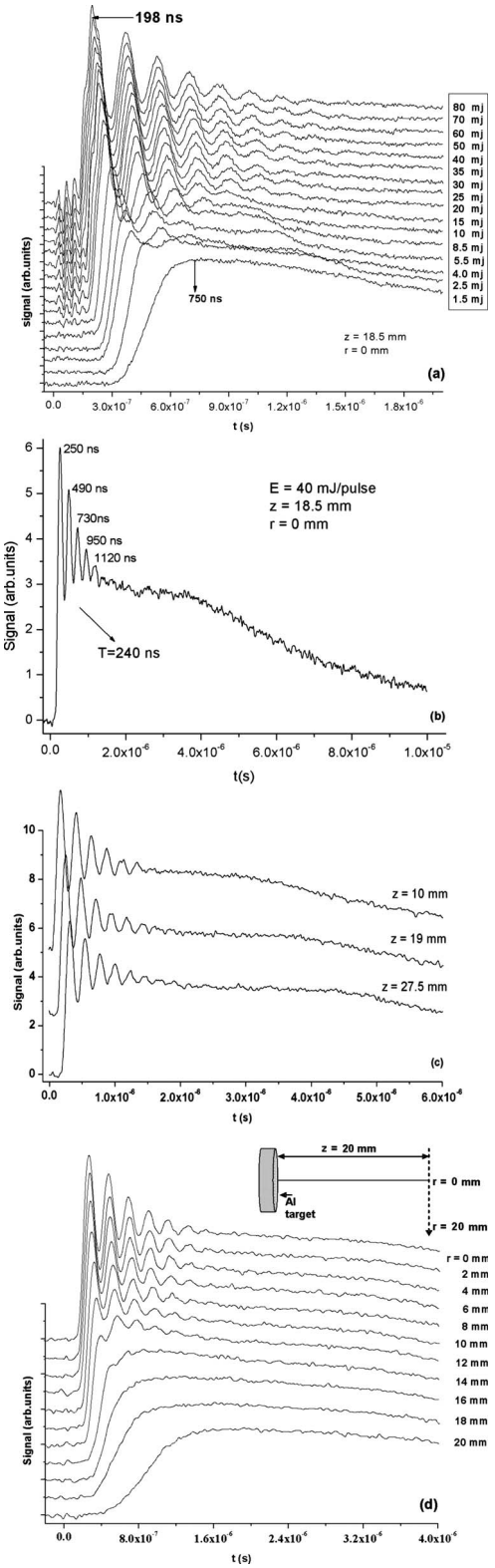

FIG. 4. (a) Transient ionic currents recorded by the Langmuir probe (placed at $z=18.5$ mm on the normal to the target) for different laser pulse energies in the range 1.5–80 mJ, (b) expanded view of (a) for 40 mJ/pulse; (c) transient ionic currents recorded by the Langmuir probe located at various distances on the normal to the target; (d) transient ionic currents recorded by the Langmuir probe keeping $z=20$ mm constant and varying the radial distance r to the expansion axis.

$$\frac{\delta \boldsymbol{V}}{dt} = \frac{\partial \boldsymbol{V}}{\partial t} + \boldsymbol{\nabla}\left(\frac{\boldsymbol{V}^2}{2}\right) - iD\Delta \boldsymbol{V} = \boldsymbol{0}, \tag{3a}$$

or, in terms of the ψ function, a Schrödinger-type equation results:

$$D^2\Delta\psi + iD\partial_t\psi = 0. \tag{3b}$$

Therefore the function ψ becomes simultaneously the wave function and the complex speed potential (for other details see [11,16]).

Let us consider the wave function, $\psi=\sqrt{\rho}e^{iS}$, with $\sqrt{\rho}$ the amplitude and S the phase of ψ. Then, the complex speed field (2) becomes

$$\boldsymbol{V} = \boldsymbol{v} + i\boldsymbol{u}, \tag{4a}$$

$$\boldsymbol{v} = 2D\,\boldsymbol{\nabla} S, \tag{4b}$$

$$\boldsymbol{u} = -D\,\boldsymbol{\nabla}\,\ln\rho. \tag{4c}$$

Introducing (4a)–(4c) in (3a) and separating the real and imaginary parts (for details on the method see [17]), we obtain

$$\frac{\partial \boldsymbol{v}}{\partial t} + \boldsymbol{\nabla}\left(\frac{\boldsymbol{v}^2 - \boldsymbol{u}^2}{2} - D\,\boldsymbol{\nabla}\cdot\boldsymbol{u}\right) = \boldsymbol{0}, \tag{5a}$$

$$\frac{\partial \boldsymbol{u}}{\partial t} + \boldsymbol{\nabla}(\boldsymbol{v}\cdot\boldsymbol{u} + D\,\boldsymbol{\nabla}\cdot\boldsymbol{v}) = \boldsymbol{0}, \tag{5b}$$

or, up to an arbitrary phase factor which may be set to zero by a suitable choice of the phase of ψ,

$$[m\partial_t\boldsymbol{v} + m(\boldsymbol{v}\cdot\boldsymbol{\nabla})\boldsymbol{v}] = -\boldsymbol{\nabla}(Q^{(2)}), \tag{6a}$$

$$\partial_t\rho + \boldsymbol{\nabla}\cdot(\rho\boldsymbol{v}) = 0, \tag{6b}$$

with $Q^{(2)}$ the fractal potential in the topological dimension $D_T=2$ (for details on the topological dimension, see [13–16]),

$$Q^{(2)} = -2mD^2\frac{\Delta\sqrt{\rho}}{\sqrt{\rho}} = -\frac{m\boldsymbol{u}^2}{2} - mD\,\boldsymbol{\nabla}\cdot\boldsymbol{u}. \tag{7}$$

The fractal potential depends only on the imaginary part $\boldsymbol{u}$ of the complex speed field $\boldsymbol{V}$ and it comes from the nondifferentiability of the fractal space-time.

Assuming that $\nabla Q^{(2)}=-(1/\rho)\nabla p$ with p the pressure (for details on this assertion see [16]), Eqs. (6a) and (6b) of the hydrodynamic model can be written in the standard form,

$$\partial_t(\rho\boldsymbol{v}) + \boldsymbol{v}\cdot\boldsymbol{\nabla}(\rho\boldsymbol{v}) = -\boldsymbol{\nabla}p, \tag{8a}$$

$$\partial_t\rho + \boldsymbol{\nabla}\cdot(\rho\boldsymbol{v}) = 0. \tag{8b}$$

Usually, for the numerical simulations, the specific internal energy e and the conservation law

$$\partial_t(\rho e) + \boldsymbol{\nabla}(\rho e\boldsymbol{v}) = -p\,\boldsymbol{\nabla}\cdot\boldsymbol{v} \tag{9}$$

must be added to the system (8a) and (8b). Details on the method of derivation of these equations are given in Ref. [26].

Formally, Eqs. (8a), (8b), and (9) are similar to the classical hydrodynamic equations used in modeling of the laser plume expansion into vacuum [5,9]. However, there is an essential difference: Eqs. (8a), (8b), and (9) are obtained using the scale relativity theory [16] in the topological dimension $D_T=2$, i.e., in a theory where the physical parameters are scale dependent. We note that in a topological dimension $D_T \neq 2$ of the scale relativity [16], the hydrodynamic equations would be totally different from Eqs. (8a), (8b), and (9).

The wave function of $\psi(r,t)$ is invariant when its phase changes by an integer multiple of 2π. Indeed, Eq. (4b) gives

$$\oint m\boldsymbol{v}\, d\boldsymbol{r} = 2mD \oint dS = 4\pi nmD, \quad n = 0, \pm 1, \pm 2, \ldots , \tag{10}$$

a condition of compatibility between the fractal scale and the nonfractal one. The set of equations (6a) and (6b) represents a complete system of differential equations for the fields $\rho(\boldsymbol{r},t)$ and $v(\boldsymbol{r},t)$; relation (10) relates each solution $(\rho,\boldsymbol{v})_n$ with the wave solution ψ in a unique way.

The field $\rho(\boldsymbol{r},t)$ is a probability distribution, namely, the probability of finding the particle in the vicinity $d\boldsymbol{r}$ of the point $\boldsymbol{r}$ at time t,

$$dP = \rho\, d\boldsymbol{r}, \tag{11a}$$

$$\int\int\int \rho\, d\boldsymbol{r} = 1, \tag{11b}$$

the space integral being extended over the entire area of the system. Any time variation of the probability density $\rho(\boldsymbol{r},t)$ is accompanied by a probability current ρv pointing toward or outward, the corresponding field point $\boldsymbol{r}$ [Eq. (6b)]. Therefore, Eq. (6b) by means of Eqs. (11a) and (11b) corresponds to the Born postulate.

The position probability of the real velocity field $v(\boldsymbol{r},t)$ [Eq. (6a)] varies with space and time similar to that of a hydrodynamic fluid placed in the fractal potential (7). The fluid (in the sense of a statistical particle ensemble) exhibits, however, an essential difference compared to an ordinary fluid [16]: in a rotation motion $v(\boldsymbol{r},t)$ increases (decreases) with the decreasing (increasing) distance $\boldsymbol{r}$ from the center [Eq. (10)].

The expectation values for the real velocity field and the velocity operator $\hat{\boldsymbol{v}} = -2iD\boldsymbol{\nabla}$ of the fractal mechanics are equal,

$$\langle \boldsymbol{v} \rangle = \int\int\int \rho\boldsymbol{v}\, d\boldsymbol{r} = \int\int\int \Psi^* \hat{\boldsymbol{v}} \Psi\, d\boldsymbol{r} = \langle \hat{\boldsymbol{v}} \rangle_{\text{wave mechanics}}, \tag{12}$$

but at higher orders, $|n|>2$, similar identities are invalid, namely, $\langle v^n \rangle \neq \langle v^n \rangle_{\text{wave mechanics}}$. The expectation for the "fractal force" vanishes at all times (theorem of Ehrenfest [27]), i.e.,

$$\langle -\boldsymbol{\nabla} Q^{(2)} \rangle = \int\int\int \rho(-\boldsymbol{\nabla} Q^{(2)}) d\boldsymbol{r} = 0, \tag{13}$$

or explicitly

$$2mD^2 \int\int\int \rho\boldsymbol{\nabla}\left(\frac{\nabla^2\sqrt{\rho}}{\sqrt{\rho}}\right) d\boldsymbol{r} = mD^2 \oint (\rho\boldsymbol{\nabla}\boldsymbol{\nabla}\ln\rho)\cdot d\boldsymbol{\sigma} = 0. \tag{14}$$

Two types of stationary states are to be distinguished.

(i) Dynamic states. For $\partial/\partial t = 0$ and $\boldsymbol{v} \neq 0$, Eqs. (6a) and (6b) give

$$\boldsymbol{\nabla}\left(\frac{1}{2}m\boldsymbol{v}^2 - \frac{m\boldsymbol{u}^2}{2} - mD\boldsymbol{\nabla}\cdot\boldsymbol{u}\right) = 0, \tag{15a}$$

$$\boldsymbol{\nabla}(\rho\boldsymbol{v}) = \boldsymbol{0} \tag{15b}$$

namely,

$$\frac{1}{2}m\boldsymbol{v}^2 - \frac{m\boldsymbol{u}^2}{2} - mD\boldsymbol{\nabla}\cdot\boldsymbol{u} = E, \tag{16a}$$

$$\rho\boldsymbol{v} = \boldsymbol{\nabla}\times\boldsymbol{F}. \tag{16b}$$

Consequently, the nonfractal inertia $m\boldsymbol{v}\cdot\boldsymbol{\nabla}\boldsymbol{v}$ and fractal force $-\nabla Q^{(2)}$ are in balance at every field point [Eq. (15a)]. The sum of the nonfractal kinetic energy $mv^2/2$ and fractal potential $Q^{(2)}$ is invariant, i.e., equal to the integration constant $E \neq E(\boldsymbol{r})$ [Eq. (16a)]. $E \equiv \langle E \rangle$ represents the total energy of the dynamic system. The probability flow density $\rho\boldsymbol{v}$ has no sources [Eq. (15b)], i.e., its streamlines are closed [Eq. (16b)].

(ii) Static states. For $\partial/\partial t = 0$ and $v = 0$, Eqs. (6a) and (6b) give

$$\boldsymbol{\nabla}\left(-\frac{m\boldsymbol{u}^2}{2} - mD\boldsymbol{\nabla}\cdot\boldsymbol{u}\right) = 0, \tag{17}$$

i.e.,

$$-\frac{m\boldsymbol{u}^2}{2} - mD\boldsymbol{\nabla}\cdot\boldsymbol{u} = E. \tag{18}$$

Thus, the fractal force, $-\nabla Q^{(2)}$ has the zero value [Eq. (17)]. The fractal potential $Q^{(2)}$ is invariant, i.e., equal to the integration constant $E \neq E(\boldsymbol{r})$ [Eq. (18)]. $E \equiv \langle E \rangle$ represents the total energy of the static system.

V. NUMERICAL SIMULATIONS OF PLASMA EXPANSION BY MEANS OF THE FRACTAL HYDRODYNAMIC MODEL

Since Eqs. (8a), (8b), and (9) of the fractal hydrodynamic in the topological dimension $D_T=2$ are identical with those of the classical hydrodynamic model, they can be applied straightforwardly to the study of the plasma expansion (for details see [5,9]). First, let us analyze the aluminum plasma charge state distribution, following the procedure from Ref. [28]. In the framework of the collision radiative model [29,30], the time-independent case is assumed. This is supported by the fact that the typical laser pulse width involved in our experiments is much longer than the time to reach the stationary state [29], or the time an ion spends in the conduction region. The fractional populations $f(Z)$ of the charge

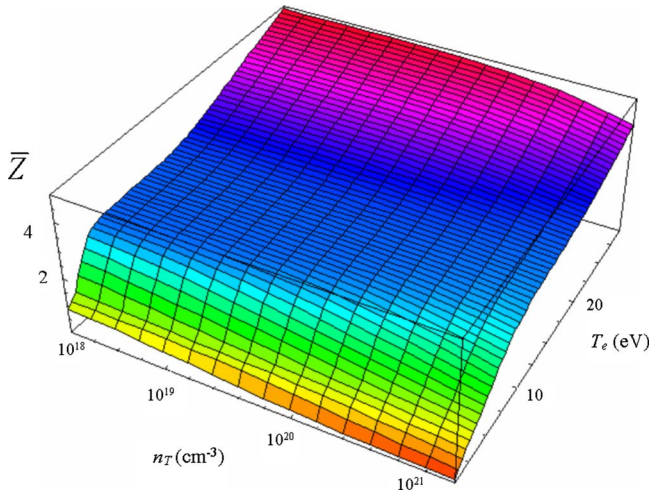

FIG. 5. (Color online) Aluminum fractional average charge state versus electron temperature and total atomic density.

states $+Z$, are connected by the simple equation system [28]

$$f(Z+1)/f(Z) = S(Z)/[\alpha_r(Z+1) + n_e\alpha_{3b}(Z+1)],$$

where n_e is the electron density, and S, α_r, and α_{3b} are the collision ionization, radiative and three-body recombination rates, respectively. These rates were calculated using the expressions given in Ref. [31] and the atomic data from the Ref. [32]. It should be noted that other processes (e.g., photoionization, photoabsorption, etc.) are neglected and only the ground states of the ions are considered. The conservation condition $\Sigma_Z f(Z)=1$ is added to obtain a nontrivial solution, and the self-consistency represented by the electron density in the equation system is eliminated by considering as an imposed parameter the total atom density n_T.

In Fig. 5 the temperature dependence of the average charge state is plotted for various total atomic densities. If we consider that the average electron temperature is given by the equation T_e (eV) $\approx 53 \times I(10^{12}$ W/cm$^2)^{0.29}$ (for details, see Refs. [30]), then for a laser beam intensity of $I \approx 5.7$ GW/cm^2, as in our experiments we obtain an electronic temperature of about $T_e \approx 11.84$ eV. According to Fig. 5, for $n_T = 10^{21}$ cm^{-3} the average charge state results as $\bar{Z} \approx 2$. We underline that T_e, n_T, and Z are average values corresponding to the plasma evolution.

Let us now apply the previous considerations in the numerical simulations of plasma expansion produced by the laser ablation. The plasma expansion has axial symmetry and is solved in the cylindrical coordinate system induced in the region above the target surface (Fig. 6). The z axis coincides with the laser beam axis and is directed along the outer normal to the target surface.

The plasma evolution is described with the following assumptions: (i) the plasma is in the state of local thermodynamical equilibrium and satisfies the quasineutrality condition; (ii) the expansion is described in the approximation of a nonviscous nonthermoconducting gas; (iii) the release of energy by thermal radiation is neglected and the ideal gas equations of state are considered; (iv) the source term is introduced through the boundary conditions. In such

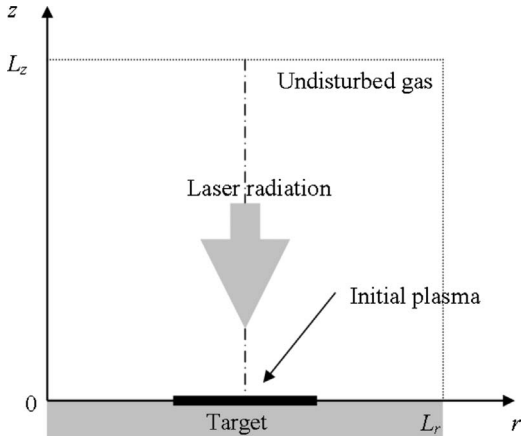

FIG. 6. Integration domain used for the numerical simulation of the laser-produced aluminum plasma expansion.

circumstances, the two-dimensional gas dynamics is described by the equation system formed by Eqs. (8a) and (8b), which are supplemented with the energy balance equation (9),

$$\frac{\partial n}{\partial t} + \frac{1}{r}\frac{\partial}{\partial r}(rnu) + \frac{\partial}{\partial z}(nv) = 0, \tag{19a}$$

$$\frac{\partial(nu)}{\partial t} + \frac{1}{r}\frac{\partial}{\partial r}(rnu^2) + \frac{\partial}{\partial z}(nuv) = -\frac{\partial p}{\partial r}, \tag{19b}$$

$$\frac{\partial(nv)}{\partial t} + \frac{1}{r}\frac{\partial}{\partial r}(rnuv) + \frac{\partial}{\partial z}(nv^2) = -\frac{\partial p}{\partial z}, \tag{19c}$$

$$\frac{\partial(ne)}{\partial t} + \frac{1}{r}\frac{\partial}{\partial r}(rnue) + \frac{\partial}{\partial z}(nve) = -p\left(\frac{1}{r}\frac{\partial(ru)}{\partial r} + \frac{\partial v}{\partial z}\right). \tag{19d}$$

Here, t is the time, r and z the spatial coordinates, n the atoms density, and u and v the velocity vector components.

For the numerical integration, the following initial and boundary conditions are taken.

(i) The box integration domain is initially filled with undisturbed gas,

$$u = v = 0, \quad n = n_0, \quad T = T_0[t = 0, 0 \leqslant (r \times z) \leqslant (L_r \times L_z)], \tag{20}$$

where T is the temperature.

(ii) The interaction of the laser beam with the target produces a plasma source located on the target surface, which is assumed to have a Gaussian space-time profile,

$$u = v = 0, \quad T = T_{\text{plasma}} \quad (z = 0), \tag{21a}$$

$$n = n_{\max} \exp\left(-\frac{(t-\tau)^2}{(\tau_L/2)^2}\right)\exp\left(-\frac{(r-L_r/2)^2}{(d_L/2)^2}\right), \tag{21b}$$

with d_L, τ_L similarly the laser beam space-time full widths, and $T_{\text{plasma}} = 11.8$ eV the initial plasma temperature. We underline that the ablation takes place only into a region with a

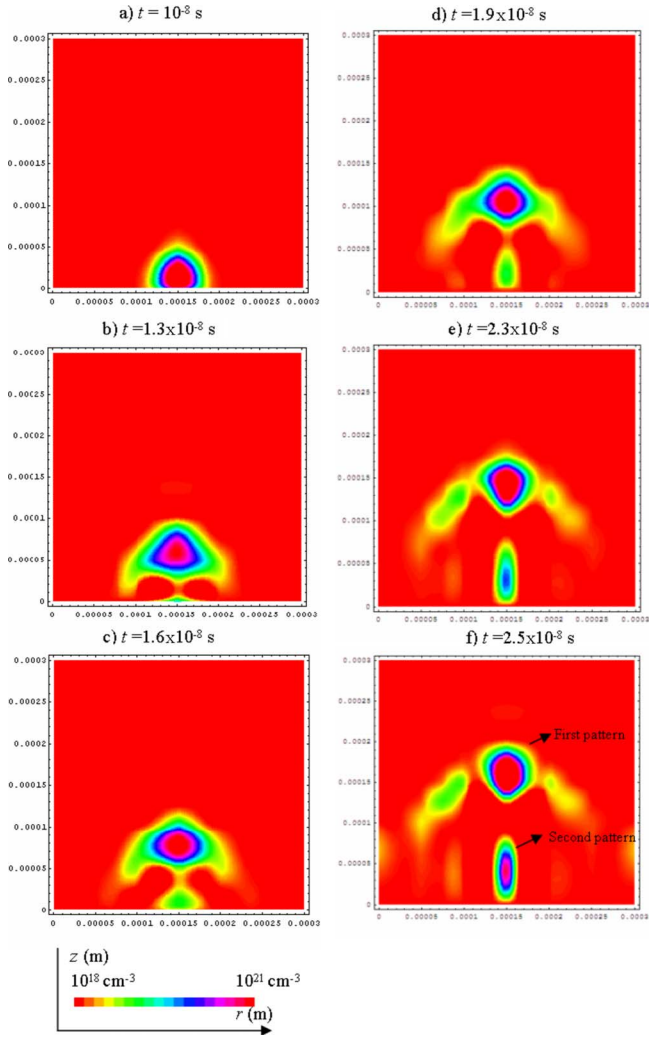

FIG. 7. (Color online) Contour plot of plasma atoms density for various time moments resulting from the numerical simulation.

characteristic diameter of about 100 μm. The maximum atom density $n_{\max}$ is taken according to the critical electron density ($n_{ec}=3.9\times10^{21}$ cm^{-3} [33]) at the laser wavelength ($\lambda=532$ nm) and the average ion charge state $\bar{Z}=2$ (for details see [30]).

(iii) The symmetry condition,

$$u(0)=u(L_r), \quad v(0)=v(L_r),$$

$$n(0)=n(L_r), \quad T(0)=T(L_r) \quad (r=0,L_r) \tag{22}$$

and the undisturbed gas is considered on the upper boundary,

$$u=v=0, \quad n=n_0, \quad T=T_0 \quad (z=L_z). \tag{23}$$

The equation system (19a)–(19d) with the conditions (20)–(23) is numerically solved using finite differences [34] and the following parameters: $L_r=L_z=300$ μm, $\tau_L=10$ ns, $d_L=100$ μm, $n_{\max}=1.95\times10^{21}$ cm^{-3}, $n_0=n_{\max}/1000$, $T_0=0.1$ eV.

In Figs. 7(a)–7(f) the two-dimensional contour curves of the total atom density at the time moments $t=$(a) 10, (b) 13, (c) 16, (d) 19, (e) 23, and (f) 25 ns are given as obtained from the numerical simulation.

The following conclusions result. (i) The plasma plume is divided into two patterns, thus reproducing the experimental observations. However, we note that our simulations were performed for a rather higher ambient gas density than that in the experiment, being limited by the accuracy of the numerical results. The influence of the vacuum chamber pressure on the plasma dynamics has been experimentally and theoretically studied [35,36], showing that the plasma splitting in the fast and lower parts is imposed by high background pressure. Our experiments show that this process also takes place at a lower pressure. (ii) Considering that the intensity of the visible light is proportional to the plasma density, a reasonable concordance between the experimental and numerical plasma shapes is evidenced.

The good agreement between experiment and theory strengthens our confidence in the capabilities of this hydrodynamic model (based on the scale relativity theory) to study dynamics of laser-produced plasmas in a more general approach.

VI. CURRENT OSCILLATIONS THROUGH THERMAL ENERGY FLUCTUATIONS

Our experimental results (the ionic current recorded by the Langmuir probe) evidenced that the first part of the transient signals has an oscillatory structure. We would like to propose a qualitative explanation of this phenomenon using the scale relativity theory [16].

Let us consider the interaction between two fractal structures, and their corresponding interface (generally, this interface delineates the double layer—see [11,12,17–19]). According to [11], the interface dynamics is described by the coupled equation set,

$$iD\frac{\partial\psi_1}{\partial t}=\lambda T_1\psi_1+\Gamma\psi_2, \tag{24a}$$

$$iD\frac{\partial\psi_2}{\partial t}=\lambda T_2\psi_2+\Gamma\psi_1 \tag{24b}$$

with ψ_1,ψ_2 the wave functions of the "plasmas," T_1, T_2 the specific temperatures of the plasmas, and λ,Γ two constants (for details about the physical significance, see Refs. [11,17,19]).

Using the wave functions $\psi_1=\sqrt{\rho_1}e^{i\Phi_1}$, $\psi_2=\sqrt{\rho_2}e^{i\Phi_2}$ and separating in (24a) and (24b) the real parts from the imaginary ones, with $\rho_1\approx\rho_2$, $\delta=\Phi_2-\Phi_1$, $T=T_2-T_1$, we obtain the current [11]

$$I=I_M\sin\left(\delta_0-\frac{\lambda}{D}\int T\,dt\right) \tag{25}$$

with δ_0 an integration constant and I_M the amplitude. Equation (25) reproduces a dc Josephson thermal type effect if $T=0$, or an ac Josephson thermal type effect if $T\neq0$, i.e., oscillations of current with the pulsation

$$\omega = \frac{\lambda T}{D}. \tag{26}$$

Since any time-dependent local thermal energy fluctuation (e.g., for the plasma expansion these fluctuations are induced by the cooling process [12]) admits a Fourier discrete decomposition [37] of the form

$$T = T_0 + \bar{T}_0 \cos(\Omega t), \quad \bar{T}_0 \ll T; \tag{27}$$

then, by substituting (27) in (25) and integrating it, the expression for the current becomes

$$I = I_M \sum_{n=-\infty}^{+\infty} (-1)^n J_n\left(\frac{\lambda \bar{T}_0}{D\Omega}\right) \sin\left[\left(n\Omega - \frac{\lambda T_0}{D}\right)t + \delta_0'\right] \tag{28}$$

where J_n is the nth-order Bessel function [37] and δ_0' a new integration constant.

When the pulsation $\Omega_0 = \lambda T_0 / D$ satisfies the relation

$$\Omega_0 = n\Omega, \tag{29}$$

the temporal average of $I = \langle I(t) \rangle$ differs from zero, i.e., there is a continuous component of the current of the form

$$I_c = (-1)^n I_M J_n\left(\frac{\lambda \bar{T}_0}{D\Omega}\right) \sin(\delta_0'). \tag{30}$$

From relation (30) peaks of the continuous current result for temperatures

$$T_n = n\bar{T}, \quad \bar{T} = D\Omega/\lambda, \quad T_n = D\Omega_0/\lambda, \quad n = 1,2, \ldots, \tag{31}$$

and consequently a negative differential conductance $dI/\lambda \bar{T}_0 < 0$—see Fig. 8. Moreover, from Eq. (30) the intensity current of the peak n varies continuously in the range of $\pm I_M J_n(\lambda \bar{T}_0 / D\Omega)$ at constant temperature $n\bar{T}$, and the phase varies in the range $-\pi/2, \pi/2$. This means that, in the interface, thermal energy is generated or absorbed. Consequently, the self-structuring of the interface as a double layer appears by means of a negative differential conductance [38–40] and, moreover, the temperature fluctuations [41] induce the current oscillations.

VII. CONCLUSIONS

The formation and dynamics of a laser-produced aluminum plasma have been experimentally studied by means of electrical and optical methods. Optically, the visible-emitting regions of the plasma form two structures with different lifetimes and expansion velocities. The results obtained by electrical probes are in good agreement with the optical observations. For example, in terms of the ionic current recorded by a Langmuir probe, the previously mentioned two-plasma structures are evidenced as two arrival times. The first part of the transient signal exhibits an oscillatory structure.

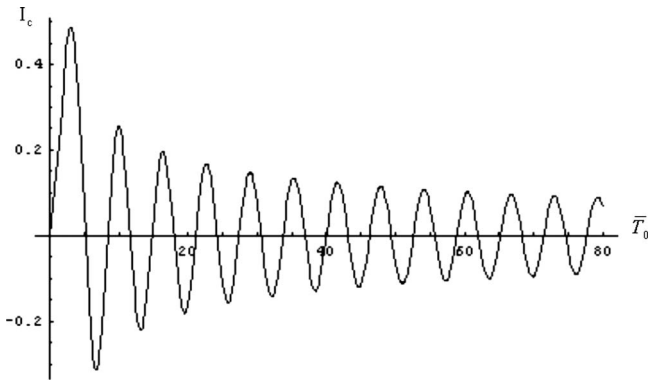

FIG. 8. Negative differential conductance, obtained by means of the negative slope of the Bessel J_3 function.

In order to reproduce the experimental observations, a hydrodynamic model in a nondifferentiable space-time has been established. By using the conservation laws of the particle number, momentum, and energy, the plasma expansion has been numerically simulated. The splitting of the plasma plume into two patterns has been successfully reproduced.

The dynamics of the plasma-plasma interface has been analyzed in an attempt to qualitatively explain the current oscillations associated with the first structure. The "transfer" through the interface replicates a dc or an ac Josephson thermal type effect. Consequently, the self-structuring of the interface as a pattern appears by means of a negative differential conductance. Moreover, the current peaks of the continuous component predicted by an ac Josephson thermal type effect can offer an explanation for the ionic current oscillations experimentally observed.

ACKNOWLEDGMENTS

The Centre d'Etudes et de Recherches Lasers et Applications is supported by the Ministère Chargé de la Recherche, the Région Nord-Pas de Calais, and the Fonds Européen de Développement Economique des Régions. Part of the present work was supported by IDEI_605 contact of CNCSIS.

[1] *Pulsed Laser Deposition of Thin Films*, edited by D. B. Chrisey and G. K. Hubler (Wiley, New York, 1994).
[2] L. J. Radziemski, Spectrochim. Acta, Part B **57**, 1109 (2002).
[3] M. F. Becker, J. R. Brock, H. Cai, D. E. Henneke, J. W. Keto, J. Lee, W. T. Nichols, and H. D. Glicksman, Nanostruct. Mater. **10**, 853 (1998).
[4] S. Ameer-Beg, W. Perrie, S. Rathbone, J. Wright, W. Weaver, and H. Champoux, Appl. Surf. Sci. **127-129**, 875 (1998).
[5] A. M. Komashko, M. D. Feit, A. M. Rubenchik, Proc. SPIE **3935**, 97 (2000).
[6] A. Bogaerts, Z. Chen, R. Gijbels, and A. Vertes, Spectrochim. Acta, Part B **58**, 1867 (2003).

[7] M. Murakami, Y. G. Kang, K. Nishihara, and H. Nishimura, Phys. Plasmas **12**, 062706 (2005).
[8] P. Mora, Phys. Rev. Lett. **90**, 185002 (2003).
[9] S. I. Anisimov, B. S. Luk'yanchuk, and A. Luches, Appl. Surf. Sci. **96-98**, 24 (1996).
[10] I. V. Nemchinov, Prikl. Mat. Mekh. **29**, 134 (1965).
[11] S. Gurlui, M. Agop, M. Strat, G. Strat, S. Bacaita, and A. Cerepaniuc, Phys. Plasmas **13**, 063503 (2006).
[12] N. M. Bulgakova, A. V. Bulgakov, and O. F. Bobrenok, Phys. Rev. E **62**, 5624 (2000).
[13] A. Le Mehante, *Les Geometries Fractales* (Hermes, Paris, 1990).
[14] J. Feder, and A. Aharony, *Fractals in Physics* (North Holland, Amsterdam, 1990).
[15] J. F. Gouyet, *Physique et Structures Fractals* (Masson, Paris, 1992).
[16] L. Nottale, *Fractal Space-Time and Microphysics: Towards a Theory of Scale Relativity* (World Scientific, Singapore, 1993).
[17] M. Agop, and I. Rusu, Chaos, Solitons Fractals **34**, 172 (2007).
[18] M. Sanduloviciu, V. Melning, and C. Borcia, Phys. Lett. A **229**, 354 (1997).
[19] T. Sato, Phys. Plasmas **3**, 2135 (1996).
[20] S. Gurlui, M. Sanduloviciu, C. Mihesan, M. Ziskind, and C. Focsa, in *Periodic Phenomena in Laser-Ablation Plasma Plumes: A Self-Organization Scenario*, edited by M. J. Sadowski, M. Dudek, H.-J. Hartfuss, and E. Pawelec, AIP Conf. Proc. No. 812 (AIP, Melville, NY, 2006), p. 279.
[21] S. Gurlui, M. Sanduloviciu, M. Strat, G. Strat, C. Mihesan, M. Ziskind, and C. Focsa, J. Optoelectron. Adv. Mater. **8**, 148 (2006).
[22] X. Xu, Appl. Surf. Sci. **197-198**, 61 (2002).
[23] X. Xu and K. H. Song, Mater. Sci. Eng., A **292** 162 (2000).
[24] K. H. Song and X. Xu, Appl. Surf. Sci. **127-129**, 111 (1998).
[25] R. Decoste and B. H. Ripin, Phys. Rev. Lett. **40**, 34 (1978).
[26] M. Agop, P. Nica, S. Gurlui, G. Strat, and M. Strat, J. Optoelectron. Adv. Mater. **10**, 1526 (2008).
[27] *Quantum Mechanics, Diffusion and Chaotic Fractals*, edited by M. S. El Naschie, O. E. Rössler, and I. Prigogine (Elservier, Oxford, 1995).
[28] P. Nica, S. Miyamoto, S. Amano, T. Inoue, A. Shinoura, K. Kaku, and T. Mochizuki, Appl. Phys. Lett. **89**, 041501 (2006).
[29] D. Colombant and G. F. Tonon, J. Appl. Phys. **44**, 3524 (1973).
[30] D. Salzman, *Atomic Physics in Hot Plasma* (Oxford University Press, New York, 1998).
[31] I. C. E. Turcu and J. B. Dance, *X-Rays from Laser Plasmas* (Wiley, Chichester, UK, 1998).
[32] R. L. Kelly, *Atomic and Ionic Spectrum Lines Below 2000 Å* (Oak Ridge National Laboratory, Oak Ridge, TN, 1982).
[33] L. Spitzer, *Physics of Fully Ionized Gases* (Wiley, New York, 1962).
[34] O. C. Zienkiewicz, and R. L. Taylor, *The Finite Element Method* (McGraw-Hill, New York, 1991).
[35] S. S. Harilal, C. V. Bindhu, M. S. Tillack, F. Najmabadi, and A. C. Gaeris, J. Appl. Phys. **93**, 2380 (2003).
[36] A. V. Bulgakov and N. M. Bulgakova, J. Phys. D **31**, 693 (1998).
[37] E. A. Jackson, *Perspectives of Non-linear Dynamics* (Cambridge University Press, Cambridge U.K., 1991), Vols. I and II.
[38] S. J. Talaşman and M. Ignat, Phys. Lett. A **301**, 83 (2002).
[39] C. Ionita, D. G. Dimitriu, and R. Schrittwieser, Int. J. Mass. Spectrom. **233**, 343 (2004).
[40] E. Lozneanu, V. Popescu, and M. Sanduloviciu, J. Appl. Phys. **92**, 1195 (2002).
[41] J. Martan, O. Cibulka, and N. Semmar, Appl. Surf. Sci. **253**, 1170 (2007).